Catalysis Today 166 (2011) 140–145

Contents lists available at ScienceDirect

Catalysis Today

journal homepage: www.elsevier.com/locate/cattod

Preparation of γ-Bi_2MoO_6 thin films by thermal evaporation deposition and characterization for photocatalytic applications

E. López Cuéllar[a,b], A. Martínez-de la Cruz[a,b,*], K.H. Lozano Rodríguez[a], U. Ortiz Méndez[a,b]

[a] Facultad de Ingeniería Mecánica y Eléctrica, Universidad Autónoma de Nuevo León, Ciudad Universitaria, C.P. 66451, San Nicolás de los Garza, N.L., Mexico
[b] Centro de Innovación, Investigación y Desarrollo en Ingeniería y Tecnología (CIIDIT), Universidad Autónoma de Nuevo León, Apodaca, N.L., Mexico

ARTICLE INFO

Article history:
Available online 9 June 2010

Keywords:
Bi_2MoO_6
Photocatalysis
Photosensitization
Thin film
Thermal evaporation

ABSTRACT

Thin films of γ-Bi_2MoO_6 were formed from γ-Bi_2MoO_6 powders by a decomposition/evaporation sequential process in a Thermal Evaporation System (TES). In order to get a controlled decomposition/evaporation of the material the deposition rate was fixed at 1.2 Å s^{-1}. The deposited films were analyzed by XRD, TEM, SEM, and EDS. These analyses revealed the formation of Bi and Mo nanoparticles of around 10 nm in their metallic form, respectively. The EDS analysis of the deposited film showed that the atomic Bi–Mo ratio (2:1) was maintained. The thin film was treated at 550 °C under atmospheric oxygen to promote the formation of γ-Bi_2MoO_6 oxide. The XRD confirmed the formation of the γ-Bi_2MoO_6 oxide in a thin film of 200 nm of thickness. Thin films of γ-Bi_2MoO_6 showed photocatalytic activity for the bleaching of rhodamine B under visible-light irradiation.

1. Introduction

The Bi_2O_3–MoO_3 binary system has a notable technological relevance due to the fact that some oxides within the system have been successfully used in industrial applications. In particular, the well-known phases α-$Bi_2Mo_3O_{12}$, β-$Bi_2Mo_2O_9$, and γ-Bi_2MoO_6 have been widely studied as selective catalysts on the oxidation and ammoxidation of lower olefins, especially for the dehydrogenation of n-butene to 1,3-butadiene [1–3].

Recently, Shimodaira et al. reported the ability of the α-$Bi_2Mo_3O_{12}$, β-$Bi_2Mo_2O_9$, and γ-Bi_2MoO_6 molybdates as photocatalysts in the O_2-evolution from an $AgNO_3$ solution by using visible-light irradiation [4]. Their work has opened a new field of application of molybdates as photocatalysts on heterogeneous photocatalytic reactions. In the last two years, several authors have reported the efficiency of the γ-Bi_2MoO_6 phase as photocatalyst on the degradation of the organic dye rhodamine B (rhB) under visible-light irradiation [5–11]. The number of published papers in the last two years revealed an increasing interest in the search of possible applications of γ-Bi_2MoO_6 as photocatalyst under visible-light irradiation.

On the other hand, worse results have been obtained when α-$Bi_2Mo_3O_{12}$ and β-$Bi_2Mo_2O_9$ are used as photocatalysts [12,13]. This situation can be associated with their crystal structure, while γ-Bi_2MoO_6 has a crystalline structure based in MoO_6 octaedra; the crystalline structures of α-$Bi_2Mo_3O_{12}$ and β-$Bi_2Mo_2O_9$ are building with MoO_4 tetraedra [4].

For this reason, several efforts have been directed to synthesize the γ-Bi_2MoO_6 oxide with a higher surface area than that obtained by the classical solid-state reaction in order to increase its catalytic activity. In this sense, the synthesis of γ-Bi_2MoO_6 has been previously reported by using organic complex precursors [5], microwave-assisted synthesis [7,9], hydrothermal synthesis [11,14,15], co-precipitation [16], and ultrasonic treatment [6]. The synthesis of γ-Bi_2MoO_6 by alternative preparation methods, such as those mentioned above, leads to the synthesis of materials with small particles and high surface areas. From the heterogeneous photocatalysis point of view, these characteristics play an important role in the degradation process. For example, the synthesis of γ-Bi_2MoO_6 by the organic complex route produced a material that reduced the half-life time of the rhB from $t_{1/2}$ = 1543 min (prepared by the solid-state reaction) to 32 min [5].

By taking into account the potential of the γ-Bi_2MoO_6 oxide as photocatalyst, recent works have reported the formation of thin films of the oxide by dip-coating and the evaluation of their photoelectrochemical properties [17–19]. The use of the photocatalyst in films instead of suspensions eliminates the complicated process of removing the photocatalyst from the solution after the pollutants have been eliminated. In this work, the possibility of obtaining thin γ-Bi_2MoO_6 oxide films by thermal evaporation deposition is analyzed. By following this route, thin films were synthesized and characterized by conventional experimental techniques. On the

* Corresponding author at: Universidad Autonoma de Nuevo Leon, Facultad de Ingenieria Mecanica y Electrica, Pedro de Alba s/n, Ciudad Universitaria, 66451 San Nicolás de los Garza, NL, Mexico. Tel.: +52 81 83 29 40 20; fax: +52 81 83 32 09 04.
E-mail address: azael70@yahoo.com.mx (A. Martínez-de la Cruz).

0920-5861/$ – see front matter © 2010 Elsevier B.V. All rights reserved.
doi:10.1016/j.cattod.2010.05.005

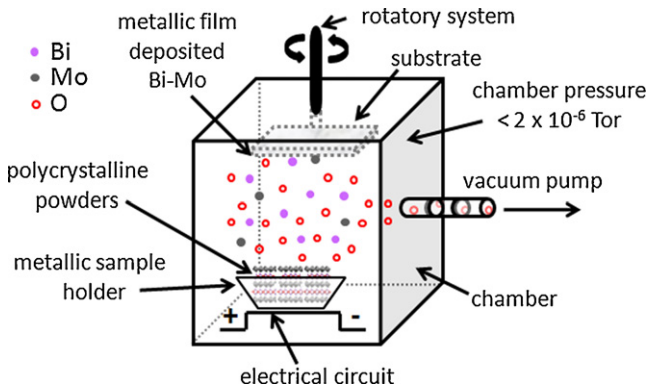

Fig. 1. Graphical scheme of the decomposition/evaporation of γ-Bi_2MoO_6 crystalline powders and deposition of metallic elements in the substrate.

basis of the results, the mechanism of formation of the γ-Bi_2MoO_6 film was elucidated. A method of rapid assessment of photocatalytic activity of the γ-Bi_2MoO_6 films was developed by placing a fine layer of rhB over the surface of the semiconductor.

2. Experimental

γ-Bi_2MoO_6 crystalline powders were used as evaporation source to produce the thin films. For this purpose, the γ-Bi_2MoO_6 oxide was synthesized by the traditional solid-state reaction between Bi_2O_3 (Aldrich, 99.9%+) and MoO_3 (Merck, 99.9%+). A stoichiometric mixture was placed into a porcelain crucible and then heated at 550 °C for 96 h to obtain the binary oxide.

The thermal evaporation of the γ-Bi_2MoO_6 powders was performed in a Thermal Evaporation Åmod 204 Series System (TES) developed by the Angstrom Engineering Company. The γ-Bi_2MoO_6 oxide was placed in a metallic crucible which was connected into the electrical circuit of the TES. Pressure inside the chamber was lower than 2×10^{-6} Torr. The TES was operated in automatic mode which means that the equipment controls the power (%*P*) passing through the Thermal Resistive Deposition Source (TRDS) by fixing the deposition rate (Å s^{-1}) of the material. The control of the deposition rate was done by controlling the current passing through the TRDS. In order to avoid an abrupt evaporation of the pristine molybdate, a low deposition rate of 1.2 Å s^{-1} was selected. A scheme of the process is showed in Fig. 1.

To study the nature of the deposit, two different kinds of substrates were used: copper grids covered with Fomvar (Ø = 3 mm) and microscope glass slides (20 mm × 60 mm). The deposition process for the copper grids was finalized when the automatic mode of the TES indicated 30 nm of thickness, while for the glass substrate, the deposition was stopped when 150–200 nm of thickness were reached. It must be noted that due to the long period of time of the process by fixing a very low deposition rate, only for the deposition in the glass substrate, the deposition process was carried out in three steps to avoid over-heating in the TES.

The morphology, structure and composition of the deposited material on the copper grids were analyzed in a JEOL 2010 transmission electron microscope (TEM) operated at 200 kV. The study of the morphology and composition of the films deposited on the glass substrate was done by scanning electron microscopy (SEM) in a FEI Nova Nano SEM operated at low vacuum. The formation process of the γ-Bi_2MoO_6 film was analyzed in a Bruker D8 Advanced diffractometer with Cu K_α radiation equipped with a Vantec high-speed detector. The X-ray diffraction data of the samples were collected in the 2θ range from 10° to 70° with a scan rate of 0.05°, 0.05 s^{-1}.

The photocatalytic experiments were performed by using a Xe lamp of 10,000 K with a luminous flux of 2100 lm as source of visible light. The emission spectrum of the Xe lamp was measured on a UV–vis spectrophotometer. A negligible contribution of UV radiation was observed ($\lambda < 390$ nm), moreover, this was filtered by a borosilicate container in a 90%. In a typical experiment 0.4 mL of a solution 0.005 M of rhB in ethanol were dispersed mechanically over the surface of the semiconductor film. The sample was dried in air at room temperature. The glass substrate containing the γ-Bi_2MoO_6/rhB films was placed vertically at 5 cm of distance from the light source. Likewise, the same volume of the rhB solution was dispersed over a glass substrate free of γ-Bi_2MoO_6, and this one was used as reference. The system was surrounded with a water jacket to maintain the reaction temperature at 25 ± 1 °C. The bleaching of rhB was followed visually by taking pictures at given time intervals.

3. Results and discussions

Fig. 2a shows the TEM micrograph of the deposited particles when a copper grid was used as substrate in the experiments. In the image, round nanoparticles between 12 and 17 nm of diameter and some smaller nanoparticles indicated with arrows can be appreciated. These smaller nanoparticles have a dot appearance and a size lower than 3 nm. When an electron diffraction test was done for the entire image a ring diffraction pattern, as shown in Fig. 2b, was obtained. The ring diffraction pattern indicates small crystals; some of them are smaller than the electron beam diameter of the TEM. Moreover, these rings can be indexed on the basis of the (1 1 0) and (2 1 1) planes of a bcc Mo crystalline structure. When the diameter of the electron beam was reduced to 5 nm to attain nano-diffraction conditions, a spot diffraction pattern was obtained, as it is shown in Fig. 2c. The nano-diffraction test was carried out to analyze the nanoparticle in the center of the image in order to obtain its crystalline structure. But as it can be seen, it is possible that more than one nanoparticle was reached by the electron beam, since a diffraction pattern with more than one orientation was obtained. The indexation of this pattern revealed that all the spots correspond to planes of the hexagonal Bi crystalline structure. On the other hand, in the same Fig. 2c, the rings of the previously observed Mo structure can be now appreciated with lower intensity, which means that during the nano-diffraction tests some Mo nanoparticles were reached. The energy dispersive X-ray analysis (EDS) shown in Fig. 2d confirms the presence of Bi and Mo, which is in agreement with the results of the TEM analysis discussed above.

The TEM results indicate that the evaporation process of the material is accompanied by the decomposition of the oxide in its corresponding elements as represented in the following chemical reaction:

$$\gamma\text{-}Bi_2MoO_6 \xrightarrow{P\approx 0} 2Bi^{o}_{(g)} + Mo^{o}_{(g)} + 3O_{2(g)} \quad (1)$$

After this process, the nanoparticles of both elements were deposited on the substrate in their metallic form. Moreover, the Bi nanoparticles seem to correspond to the big ones giving spot diffraction patterns, while the Mo nanoparticles seem to be the smallest with dot shapes. These different sizes could be attributed to the difference in the melting point (mp) for both elements. The mp of Bi and Mo are 271 and 2610 °C, respectively. This enormous difference in the mp can be the origin of that Bi nanocrystals are bigger that those Mo. This could be explained as follows: when the Mo evaporated get contact with the substrate which has a surface temperature of ~80 °C, the Mo will transform in solid phase, but the size of crystal will rapidly stop to growth because the difference between the surface temperature (80 °C) and the grain growth temperature which is related to the mp (2610 °C) is very important, while for the Bi, this difference is lower, giving more chance to form bigger crystals. In a previous work the formation of reduced species

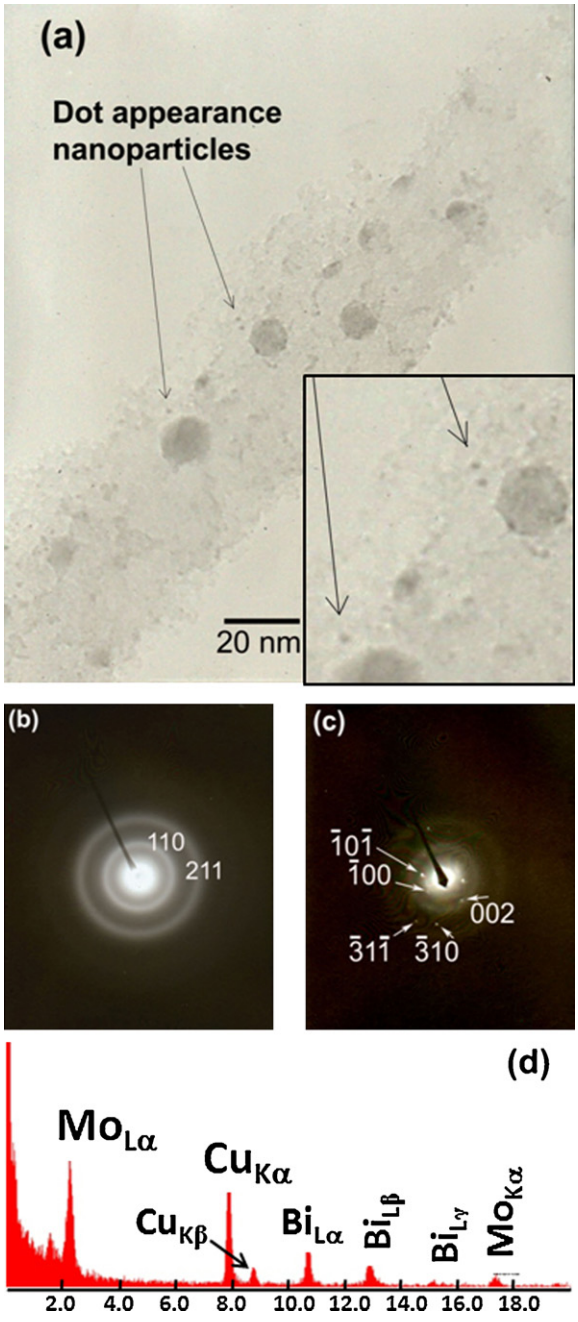

Fig. 2. TEM image (a) and diffraction patterns (b and c) of deposited nanoparticles in the copper grids, and EDS analysis (d).

during the thermal evaporation of TiO_2 was reported, including the formation of Ti metallic [20].

Fig. 3 shows a photograph of the glass substrate without treatment (a), after the material was deposited (b) and after the thermal treatment of the film (c). The glass substrate containing the deposited material, but without thermal treatment, has a dark metallic appearance, which is in agreement with the results obtained by the TEM analysis that indicates the presence of a metallic deposit. To achieve the formation of the γ-Bi_2MoO_6 oxide on the glass substrate, the film was heated at 550 °C for 24 h under atmospheric oxygen. The result of the thermal treatment was a remarkable color change from dark to pale yellow. This color could be linked to the yellow color of the γ-Bi_2MoO_6 oxide.

This assumption was validated by the X-ray diffraction (XRD) experiments. Fig. 4 shows the XRD patterns of the γ-Bi_2MoO_6 powders obtained by solid-state reaction (a), the residue powders of γ-Bi_2MoO_6 after the evaporation took place (b), the thin film deposited on the glass substrate (c), and the same thin film, but after the thermal treatment at 550 °C has been performed (d). Firstly, it can be seen that the diffraction line intensities of the powdered materials (Fig. 4a and b) are higher than those of the thin films (Fig. 4c and d) due to differences in their crystallinity degree. Now, as it can be seen in Fig. 4a, the XRD pattern of the pristine oxide powders obtained by solid-state reaction corresponds to the structure of γ-Bi_2MoO_6 (JCPDS Card No. 84-0787). The XRD pattern of the residue powders obtained during the material evaporation process indicates the presence of γ-Bi_2MoO_6 and H-Bi_2MoO_6 (JCPDS Card No. 82-2067), which means that during the evaporation conditions, γ-Bi_2MoO_6 undergoes a phase transition to its high temperature polymorph (H-Bi_2MoO_6), see Fig. 4b. These results indicate that although the source evaporation material experiments a phase transition, the chemical composition of the material keeps unaltered (atomic ratio: 2Bi, Mo, 6O). The formation and deposition of

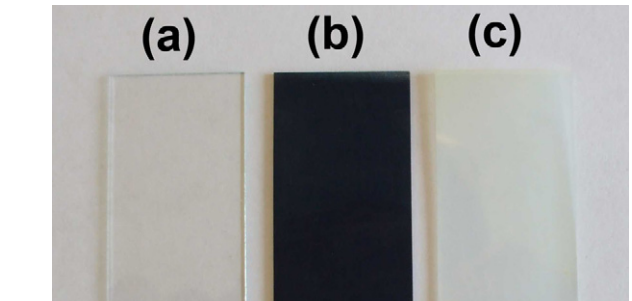

Fig. 3. Photograph of the glass substrate alone (a), the deposit on the glass substrate without heat treatment (b), and the deposit with the heat treatment (c).

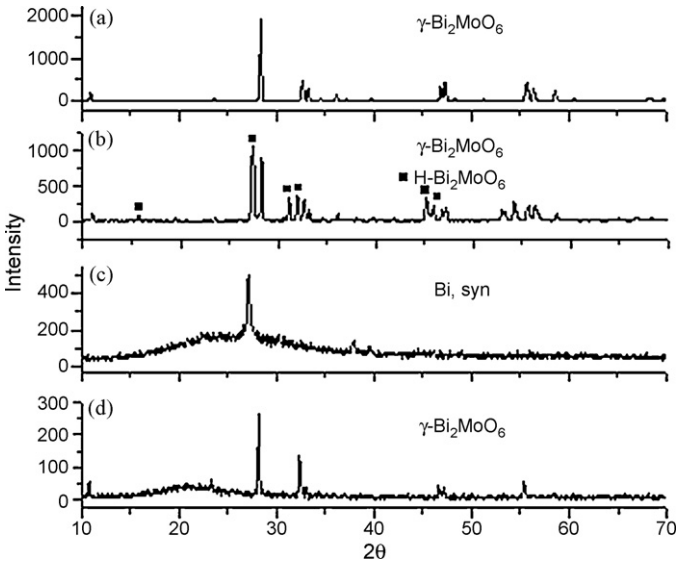

Fig. 4. XRD of γ-Bi_2MoO_6 powders obtained by solid-state reaction (a), the residue powders of γ-Bi_2MoO_6 (b), the thin metallic film deposited on glass substrate (c), and the thin film after been heat treatment with the formation of γ-Bi_2MoO_6 (d).

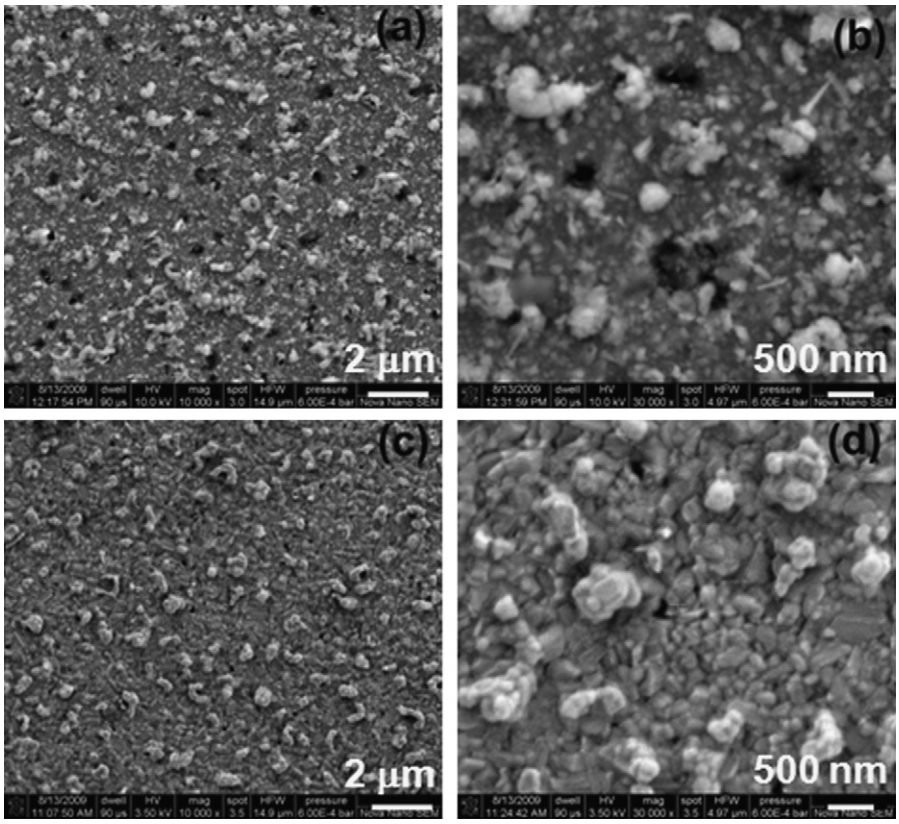

Fig. 5. SEM images of the thin metallic film on glass substrate without heat treatment (a and b), and the thin film after been heat treatment with the formation of γ-Bi_2MoO_6 (c and d).

metallic Bi was confirmed by the XRD experiments over the glass substrate, whereas evidence of the formation of metallic Mo was not observed (Fig. 4c). This fact can be due to the small thickness of the film (~200 nm). The Bi metallic structure (JCPDS Card No. 44-1246) corresponds to the structure observed previously during the TEM analysis. Finally, when the film was thermally treated under atmospheric oxygen the formation of the γ-Bi_2MoO_6 oxide was observed in pure form, see Fig. 4d.

The morphology of the thin films deposited on the glass substrate was also analyzed by SEM. Fig. 5 presents the SEM images of the thin film deposited on the glass substrate (Fig. 5a and b) and the images of the same thin film after the thermal treatment (Fig. 5c and d). In both cases at low magnification (Fig. 5a and c), a complete covered surface of the glass substrate can be observed, although the film without heat treatment shows a more porous surface. This is confirmed when the magnification is increased as it is shown in Fig. 5b–d. At a higher magnification, in Fig. 5d, a more dense image is observed with a pore size <100 nm for the thermally treated surface while the surface without heat treatment shows and increase in the number of pores and in the pore size (from ~100 to 200 nm) in Fig. 5b. The atomic relation Bi/Mo of the film obtained by EDS was 2.18 which is very close to the expected powder relation of 2.

The photocatalytic activity of γ-Bi_2MoO_6 films was tested in the bleaching of a layer of rhB dye deposited over the photocatalyst surface. In the past, some methods for assessing the photocatalytic activity of TiO_2 films under UV-irradiation were reported. For example, for this purpose a thin layer of stearic acid was deposited on the film of semiconductor and its photocatalytic destruction was monitored by FTIR [21,22]. More recently, Mills et al. reported a method based in the coloration developed by the resazurin (Rz) dye in its reduced and oxidized forms in the presence of glycerol under UV-irradiation [23]. Taking into account the photocatalytic properties of γ-Bi_2MoO_6 under visible-light irradiation for the degradation of rhB [5], this organic dye was applied as a thin layer over the photocatalyst surface. Fig. 6 shows the evolution of the color intensity of the rhB layer deposited after different times of visible-light irradiation. As it can be seen in the pictures in Fig. 6a, the rhB color fades considerably after 2 h indicating an effective bleaching of the organic dye, and after 6 h of light irradiation the glass substrate was totally bleached. A similar experiment was performed but without the photocatalyst film, as it is shown in Fig. 6b. A slow bleaching of the glass substrate was observed due to a photolysis process of the organic dye. The characteristic pink color of rhB was observed even at 32 h of visible-light irradiation. This situation indicates that the photocatalyst/visible-light irradiation combination was necessary to eliminate the organic dye layer. The marked change of color observed within the first 2 h in the experiment without photocatalyst was associated with a drying process of the film by the elimination of residual ethanol.

The bleaching of rhB by γ-Bi_2MoO_6/visible-light irradiation takes place by means of a photosensitization process where the light irradiation excites an electron from the dye layer and then it is injected into the conduction band of the semiconductor layer with the concomitant oxidation of the organic dye. This statement is based on previous studies about the photocatalytic degradation of rhB by γ-Bi_2MoO_6 nanoparticles dispersed in the solution [5]. The photosensitization process by rhB can be described in the case of the thin film of γ-Bi_2MoO_6 as follows:

$$\mathrm{rhB} + h\nu \rightarrow \mathrm{rhB}* \quad (2)$$

$$\mathrm{rhB}* + \gamma\text{-}\mathrm{Bi_2MoO_6} \rightarrow \mathrm{rhB}^{\bullet+} + \gamma\text{-}\mathrm{Bi_2MoO_6}(\mathrm{e}^-) \quad (3)$$

$$\gamma\text{-}\mathrm{Bi_2MoO_6}(\mathrm{e}^-) + \mathrm{O_2} \rightarrow \gamma\text{-}\mathrm{Bi_2MoO_6} + {}^{\bullet}\mathrm{O_2}^- \quad (4)$$

$$\mathrm{rhB}^{\bullet+} + {}^{\bullet}\mathrm{O_2}^- \rightarrow \text{subproducts} \quad (5)$$

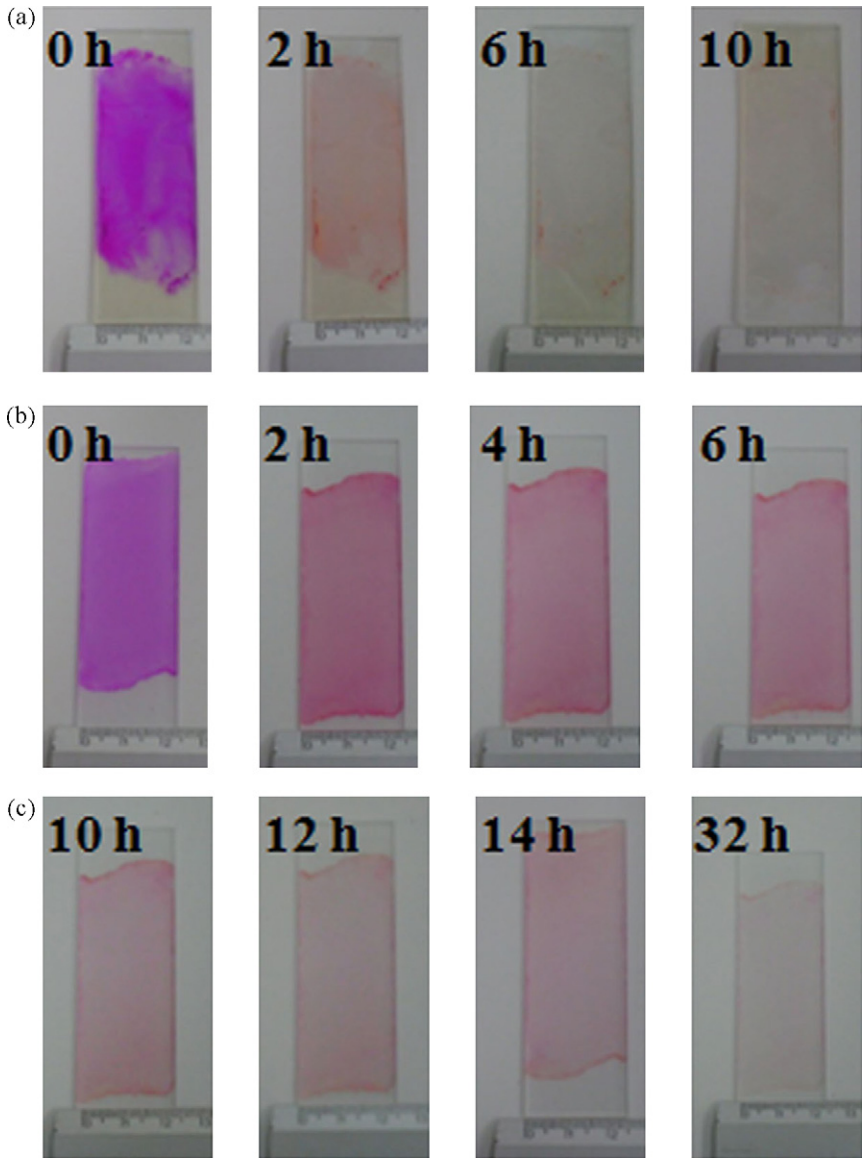

Fig. 6. Evolution of the color of a rhB thin layer over the photocatalyst film at given time intervals under visible-light irradiation (a), and an experiment performed without photocatalyst (b). (For interpretation of the references to color in this figure legend, the reader is referred to the web version of the article.)

Some experiments to elucidate the overall mechanism of bleaching of rhB in the presence of γ-Bi_2MoO_6 thin film, and the nature of the reaction intermediates are now in progress.

Due to the photocatalytic activity previously reported for γ-Bi_2MoO_6 in the degradation of organic dyes, the use of the photocatalyst in thin films instead of dispersed forms is interesting because it eliminates the complicated process of removing the photocatalyst from the treated solution.

4. Conclusions

γ-Bi_2MoO_6 thin films were formed by a decomposition/evaporation sequential process starting from γ-Bi_2MoO_6 powder previously obtained by solid-state reaction. The evaporation process of the material was controlled employing a deposition rate of 1.2 Å s^{-1}. The TEM analysis revealed that the deposited material (before the thermal treatment) was composed by nanoparticles with an average diameter of 12–17 nm, whose chemical analysis by EDS revealed that they were formed by Bi and Mo in their metallic forms.

The thin deposited film was thermally treated at 550 °C to promote the reaction of the elements (Bi and Mo) with atmospheric oxygen. The X-ray diffraction patterns confirmed the formation of the γ-Bi_2MoO_6 oxide and the SEM analysis showed the formation of a thin film with a porous surface. The thickness of the formed film was 150–200 nm. The photocatalytic activity of the semiconductor film was evaluated on the bleaching of a rhodamine B. For this purpose, a method of rapid assessment of photocatalytic activity of the γ-Bi_2MoO_6 films was developed by placing a fine layer of rhodamine B over the surface of the semiconductor.

Acknowledgements

We wish to thank CONACYT for the 82515, 81546, and 104310 projects support. We also want to thank to CIDIIT (UANL) and Departamento de Ecomateriales y Energía-Facultad de Ingeniería Civil (UANL) for its technical assistance during this work.

References

[1] Ph.A. Batist, J.F.H. Bouwens, G.C.A. Schuit, J. Catal. 25 (1972) 1.
[2] M.M. Bettahar, G. Costentin, L. Savary, J.C. Lavalley, Appl. Catal. A 145 (1996) 1.

[3] J. Jung, H. Kim, Y. Chung, T. Kim, S. Lee, S. Oh, Y. Kim, I. Song, J. Mol. Catal. A: Chem. 264 (2007) 237.
[4] Y. Shimodaira, H. Kato, H. Kobayashi, A. Kudo, J. Phys. Chem. B 110 (2006) 17790.
[5] A. Martínez-de la Cruz, S. Obregón Alfaro, E. López Cuéllar, U. Ortiz Méndez, Catal. Today 129 (2007) 194.
[6] L. Zhou, W. Wang, L. Zhang, J. Mol. Catal. A: Chem. 268 (2007) 195.
[7] J. Bi, L. Wu, J. Li, Z. Li, X. Wang, X. Fu, Acta Mater. 55 (2007) 4699.
[8] L. Xie, J. Ma, G. Xu, Mater. Chem. Phys. 110 (2008) 197.
[9] H. Xie, D. Shen, X. Wang, G. Shen, Mater. Chem. Phys. 110 (2008) 332.
[10] X. Zhao, T. Xu, W. Yao, Y. Zhu, Appl. Surf. Sci. 255 (2009) 8036.
[11] C. Xu, D. Zou, L. Wang, H. Luo, T. Ying, Ceram. Int. 35 (2009) 2099.
[12] A. Martínez-de la Cruz, S.M.G. Marcos Villarreal, M. Leticia, E. Torres-Martínez, U. López Cuéllar, Ortiz Méndez, Mater. Chem. Phys. 112 (2008) 679.
[13] A. Martínez-de la Cruz, L.G. Gracia Lozano, React. Kinet. Mech. Catal. 99 (2010) 209.
[14] H. Li, C. Liu, K. Li, H. Wang, J. Mater. Sci. 43 (2008) 7026.
[15] H. Li, K. Li, H. Wang, Mater. Chem. Phys. 116 (2009) 134.
[16] J. Jung, H. Kim, A. Choi, Y. Chung, T. Kim, S. Lee, S. Oh, I. Song, Catal. Commun. 8 (2007) 625.
[17] X. Zhao, J. Qu, H. Liu, C. Hu, Environ. Sci. Technol. 41 (2007) 6802.
[18] Y. Man, R. Zong, Y. Zhu, Acta Phys.-Chim. Sin. 23 (11) (2007) 1671.
[19] X. Zhao, T. Xu, W. Yao, Y. Zhu, Thin Solid Films 517 (2009) 5813.
[20] H.K. Pulker, G. Paesold, E. Ritter, Appl. Opt. 15 (1976) 2986.
[21] S. Sitkiewitz, A. Heller, New J. Chem. 20 (1996) 233.
[22] P. Sawunyama, L. Jiang, A. Fujishima, K. Hashimoto, J. Phys. Chem. B 101 (1997) 11000.
[23] A. Mills, J. Wang, M. McGrady, J. Phys. Chem. B 110 (2006) 18324.